Supporting information

Tungsten-modified MXene-integrated Spinel Oxides as High-Performance and Stable Catalysts for Water/Seawater Oxidation

Deepika Tanwar, P. Vignesh Raja, Padinjarethil Vishnu, and Ijjada Mahesh*

Department of Chemical Engineering,
Indian Institute of Science Education and Research Bhopal,
Madhya Pradesh - 462066, India.
*E-mail: mahesh@iiserb.ac.in; mahesh.ijjada@gmail.com

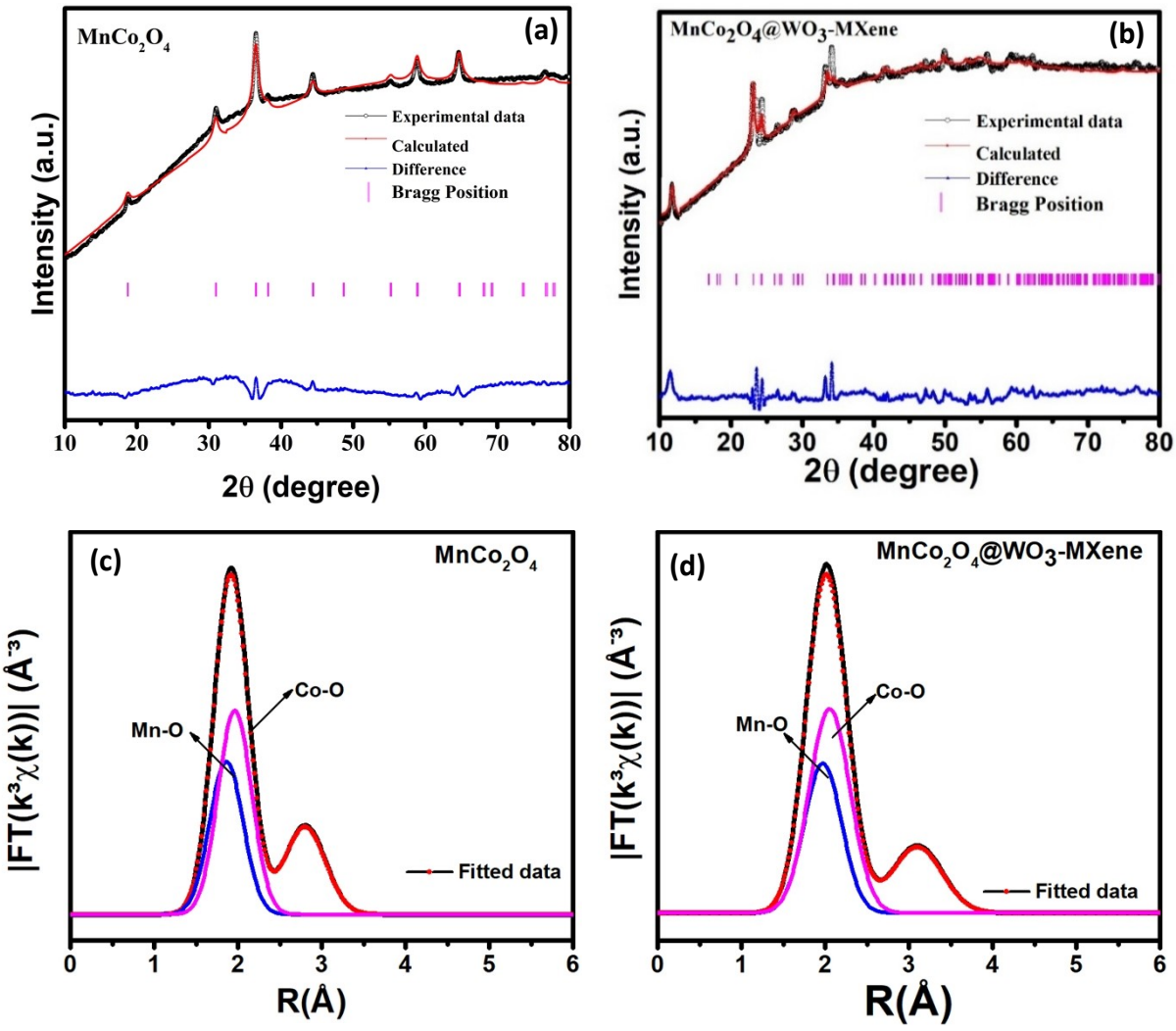

Figure S1. Rietveld refinement X-ray diffraction pattern of (a) $MnCo_2O_4$ (b) $MnCo_2O_4$-WO_3-MXene; FT fitting curves of (c) $MnCo_2O_4$ and (d) $MnCo_2O_4$-WO_3-MXene at the k^3-weighted Co K-edge EXAFS.

Table S1: Rietveld refined **s**tructural parameter of $MnCo_2O_4$ and $MnCo_2O_4$-WO_3-MXene

	$MnCo_2O_4$	**$MnCo_2O_4$-WO_3-MXene**
Lattice parameters a	8.15647	8.7900
b	8.15647	8.7900
c	8.15647	8.7900
Unit cell volume (Å^3)	542.622	679.151
Goodness of fit Chi	2.19	1.18
Bond Type	**Bond length**	
Mn-O	1.6 A^0	2.03 A^0
Co-O	1.97 A^0	2.04 A^0
Ti-C	-	1.89 A^0
W-O	-	1.7 A^0

Table S2: BET surface area and pore size distribution of the as-prepared samples

Compound	BET surface area ($m^2 g^{-1}$)	Pore Size (nm)	Pore volume (cm^3/g)
$MnCo_2O_4$	55.21	0.98	0.3534
$MnCo_2O_4$-WO_3-MXene	76.21	0.65	0.429

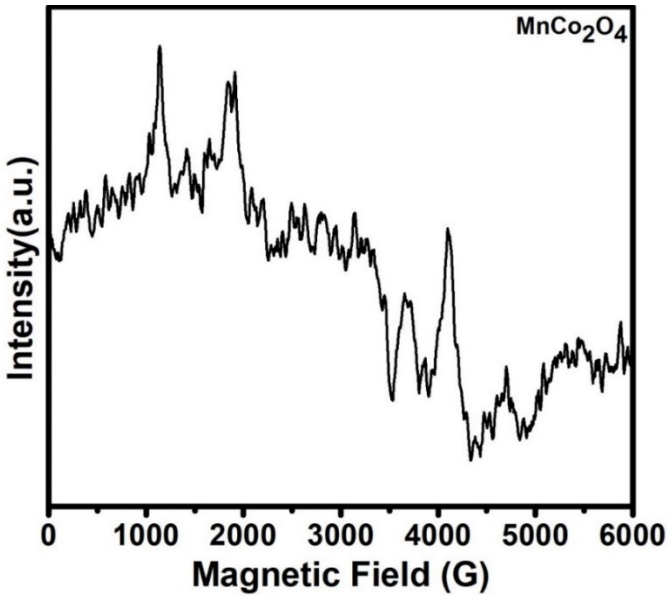

Figure S2. EPR spectra of $MnCo_2O_4$

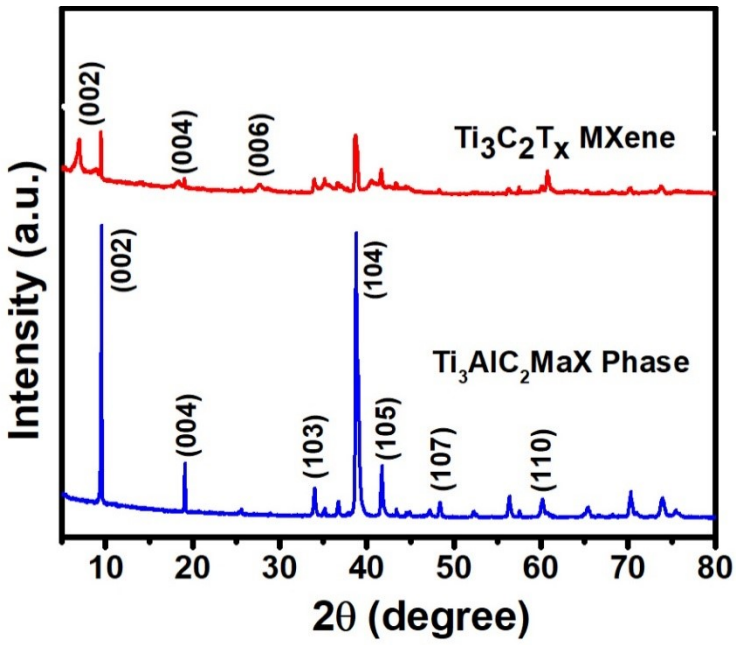

Figure S3. XRD spectra of MXene.

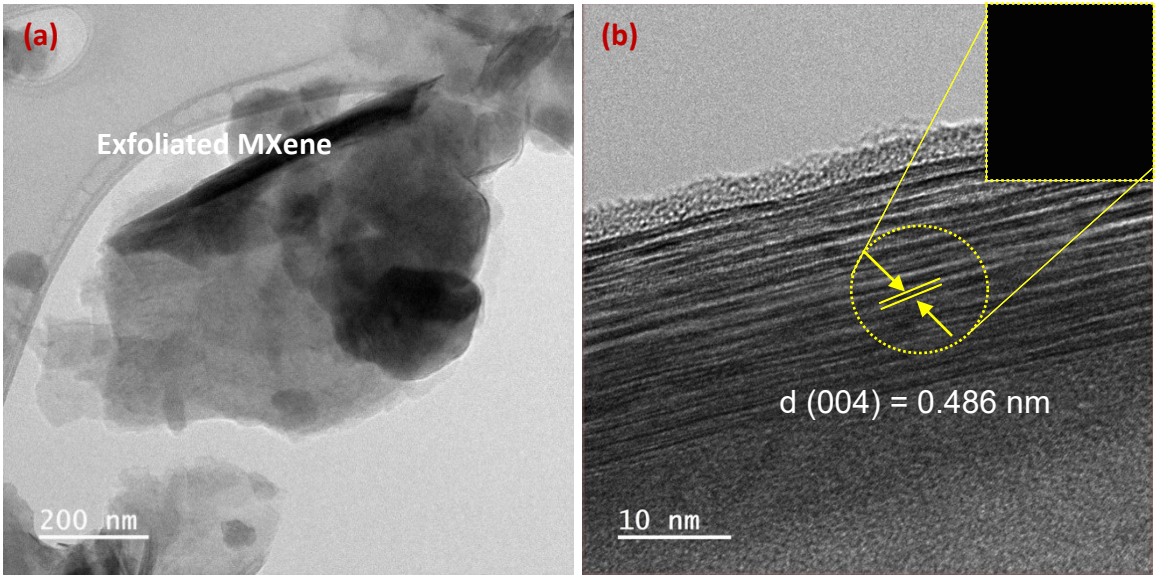

Figure S4. HRTEM image of MXene at (a) 200 nm, (b) 10 nm

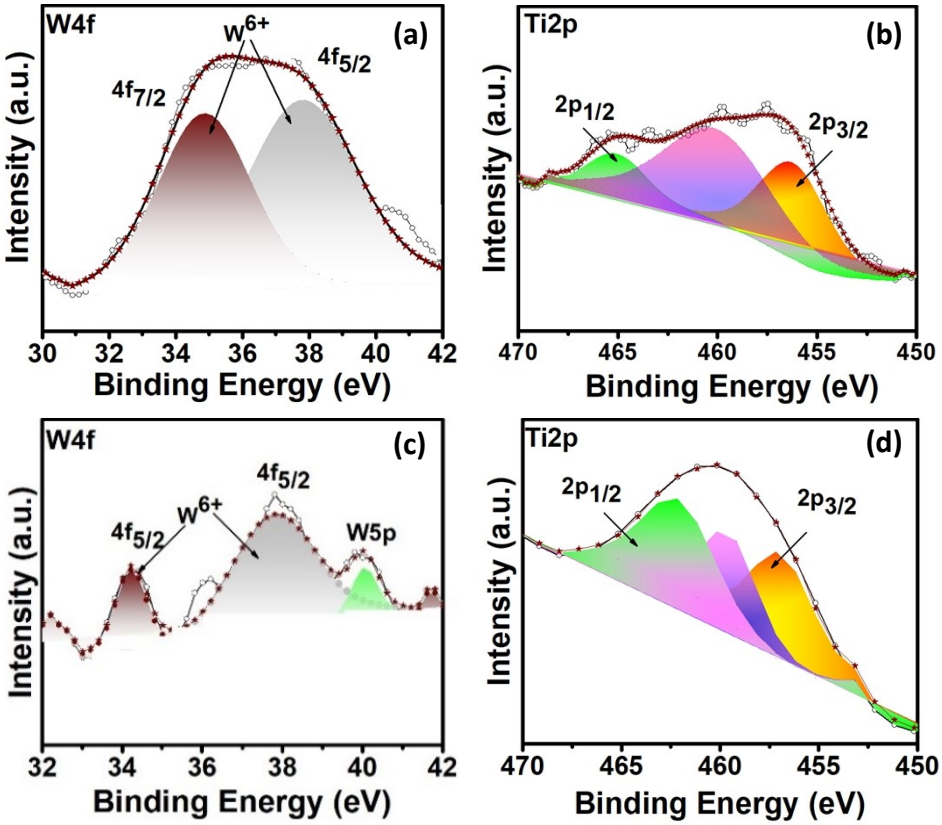

Figure S5. XPS spectra of $MnCo_2O_4$-WO_3-MXene (a) W4f, (b) Ti2p (before), (c) W4f, (d) Ti2p (after)

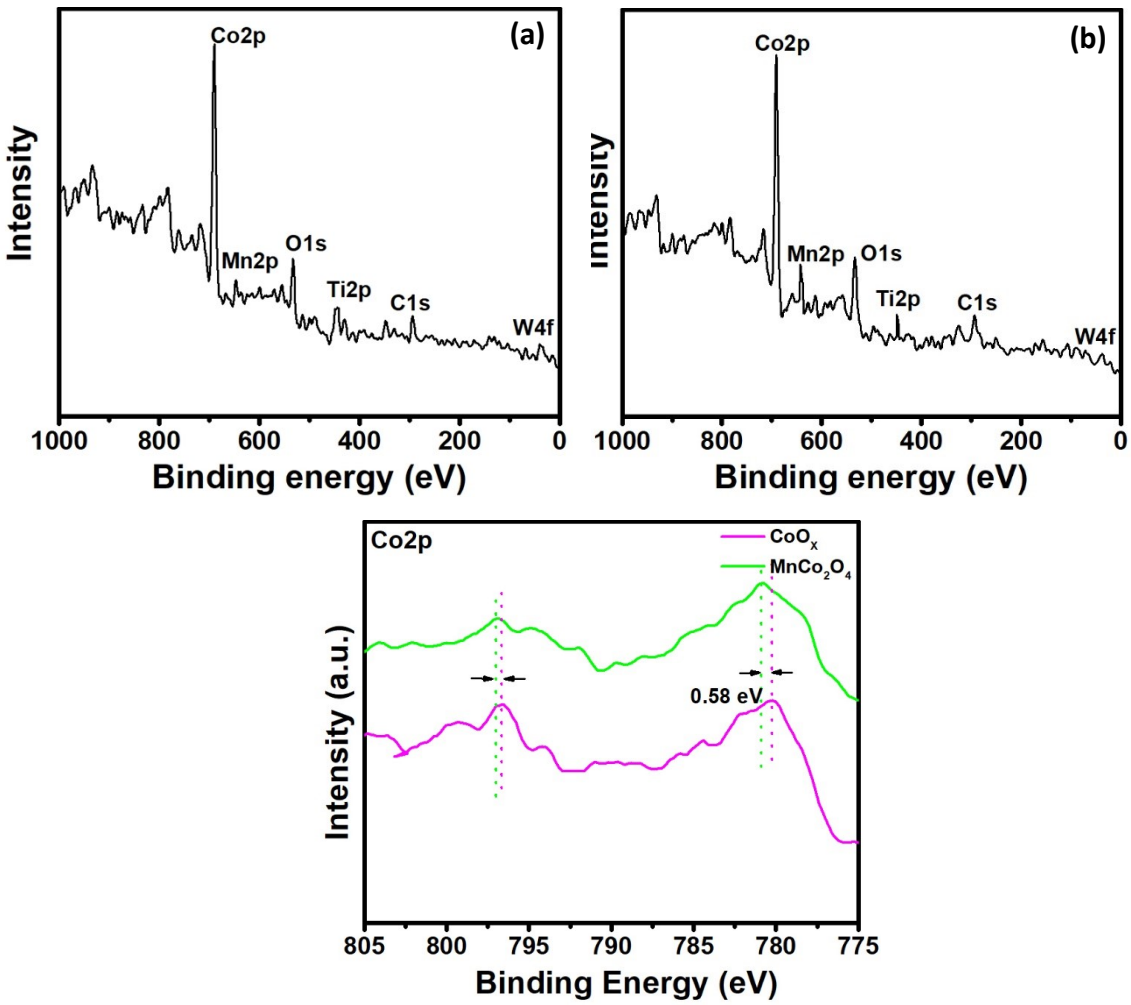

Figure S6. XPS survey spectra of $MnCo_2O_4$-WO_3-MXene (a) before, (b) after stability test, (c) Co2p XPS spectra of CoOx and MnCo2O4

Table S3: XPS Mn2p and Co2p peak data of $MnCo_2O_4$-WO_3-MXene and $MnCo_2O_4$ before testing

Samples	Peak	Oxidation state	Peak position (eV)	Average oxidation state
$MnCo_2O_4$-WO_3-MXene	Mn2p3/2	Mn^{3+} Mn^{2+}	643.12 641.77	+2.4
	Co2p3/2	Co^{3+} Co^{2+}	779.75 782.70	+2.5
	Co2p1/2	Co^{3+} Co^{2+} (Sat.)	794.80 797.48 801.70	
$MnCo_2O_4$	Mn2p3/2	Mn^{3+} Mn^{2+}	643.29 642.05	+2.3
	Co2p3/2	Co^{3+} Co^{2+} (Sat.)	778.66 780.85 788.92	+2.41
	Co2p1/2	Co^{2+} Co^{3+}	797.88 794.82	

Table S4: XPS Mn2p and Co2p peak data of $MnCo_2O_4$-WO_3-MXen after testing

Samples	Peak	Oxidation state	Peak position (eV)	Average oxidation state
$MnCo_2O_4$-WO_3-MXene	Mn2p3/2	Mn^{3+} Mn^{2+}	643.00 642.05	+2.68
	Mn2p1/2	-	653.92	
	Co2p3/2	Co^{3+} Co^{2+} (Sat.)	778.60 782.26 784.38	+2.78
	Co2p1/2	Co^{3+} Co^{2+}	793.98 796.33	

Table S5: XPS analysis results of the as-prepared samples

Compound	Co^{3+}/Co^{2+}	Mn^{3+}/Mn^{2+}	O_V/ O_{latt}
$MnCo_2O_4$	0.72	0.28	0.45
$MnCo_2O_4$-WO_3-MXene (before)	0.91	0.47	2.66
$MnCo_2O_4$-WO_3-MXene (after 100 h stability test)	2.78	2.19	2.65

Table S6: XPS W4f peak data of $MnCo_2O_4$-WO_3-MXene before and after testing

Samples		Peak	Oxidation state	Peak position (eV)
$MnCo_2O_4$-WO_3-MXene	Before	W4f7/2	W^{6+}	34.2
		W4f5/2		37.7
	After	W4f7/2	W^{6+}	34.4
		W4f5/2		37.8
		W5p	-	40.04

Table S7: XPS TiO_2 peak data of $MnCo_2O_4$-WO_3-MXene before and after testing

Samples		Peak	Peak position (eV)	Oxidation state
$MnCo_2O_4$-WO_3-MXene	Before	Ti2p3/2	456.19 459.72	Ti^{3+} Ti^{2+}
		Ti2p1/2	465.07	-
	After	Ti2p3/2	456.87 459.89	Ti^{3+} Ti^{2+}
		Ti2p1/2	462.05	-

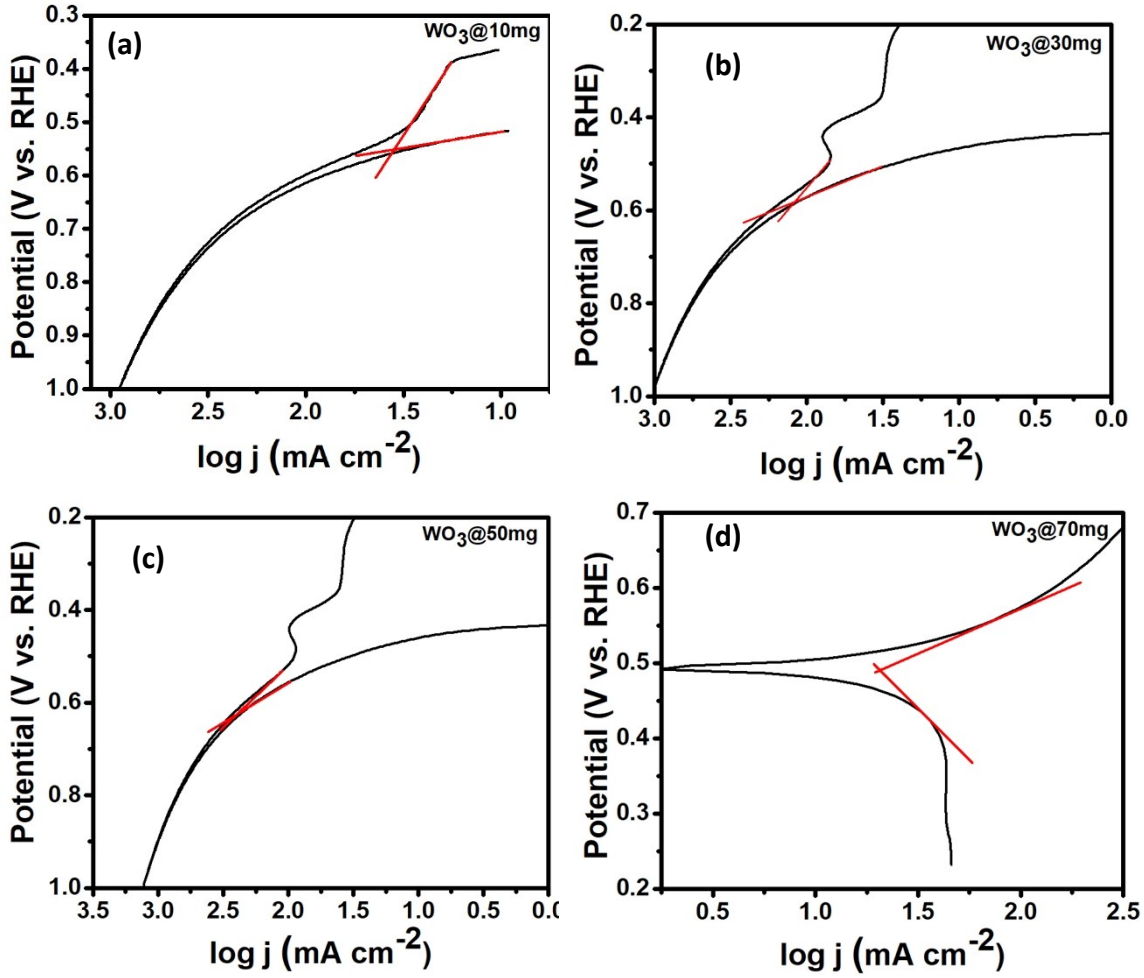

Figure S7. Corrosion test of $MnCo_2O_4$-WO_3-MXene at different concentrations of WO_3

Table S8: Corrosion current density at different concentrations of WO_3

S.N.	WO_3 loading (mg)	Corrosion current density ($\mu A\ cm^{-2}$)
1	0.1	38.97
2	0.3	7.24
3	0.5	5.18
4	0.7	29.51

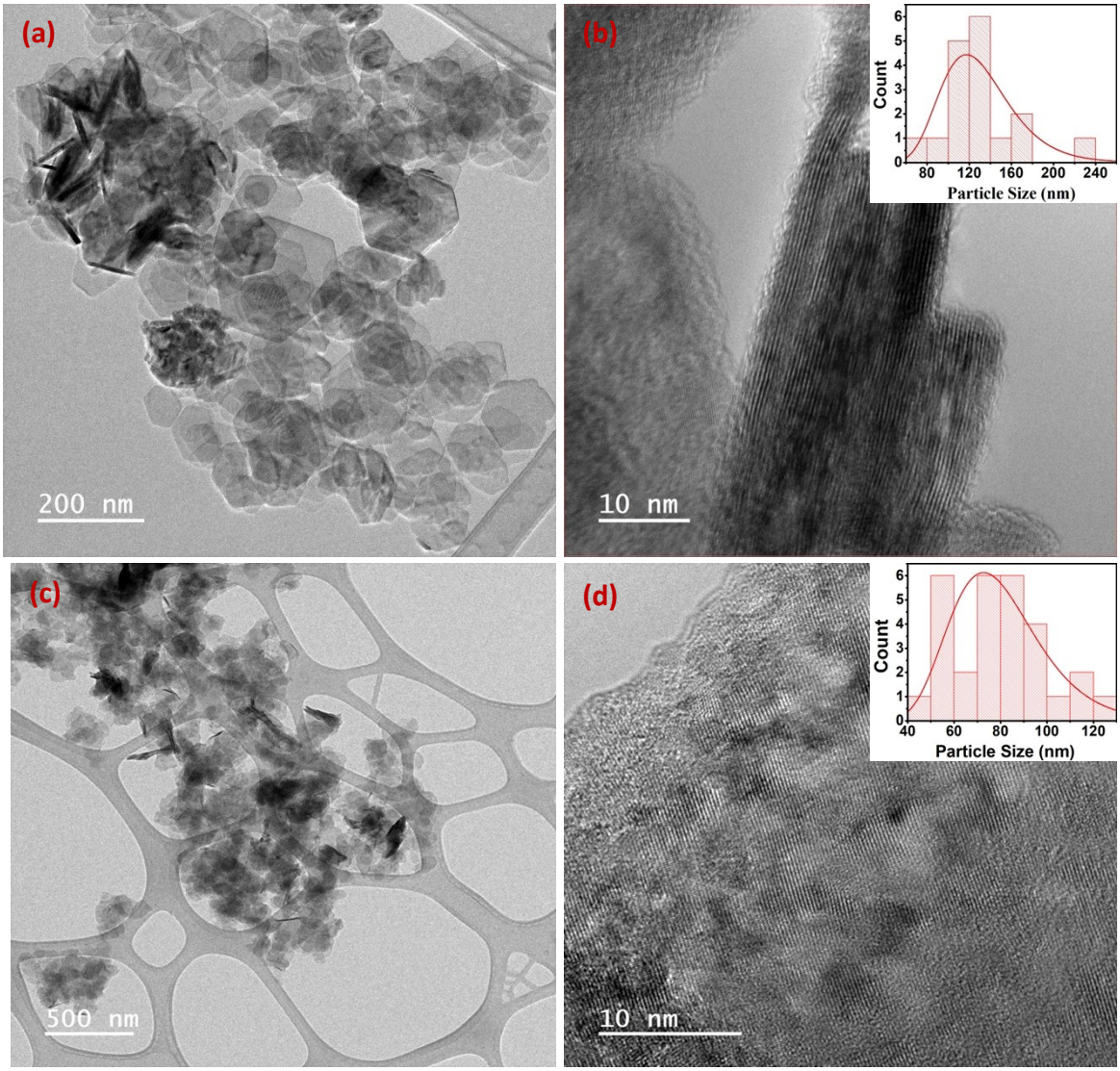

Figure S8. HRTEM image of $MnCo_2O_4$-WO_3-MXene without CTAB at (a) 200 nm, (b) 10 nm and $MnCo_2O_4$-WO_3-MXene with CTAB at (c) 500 nm, (d) 10 nm

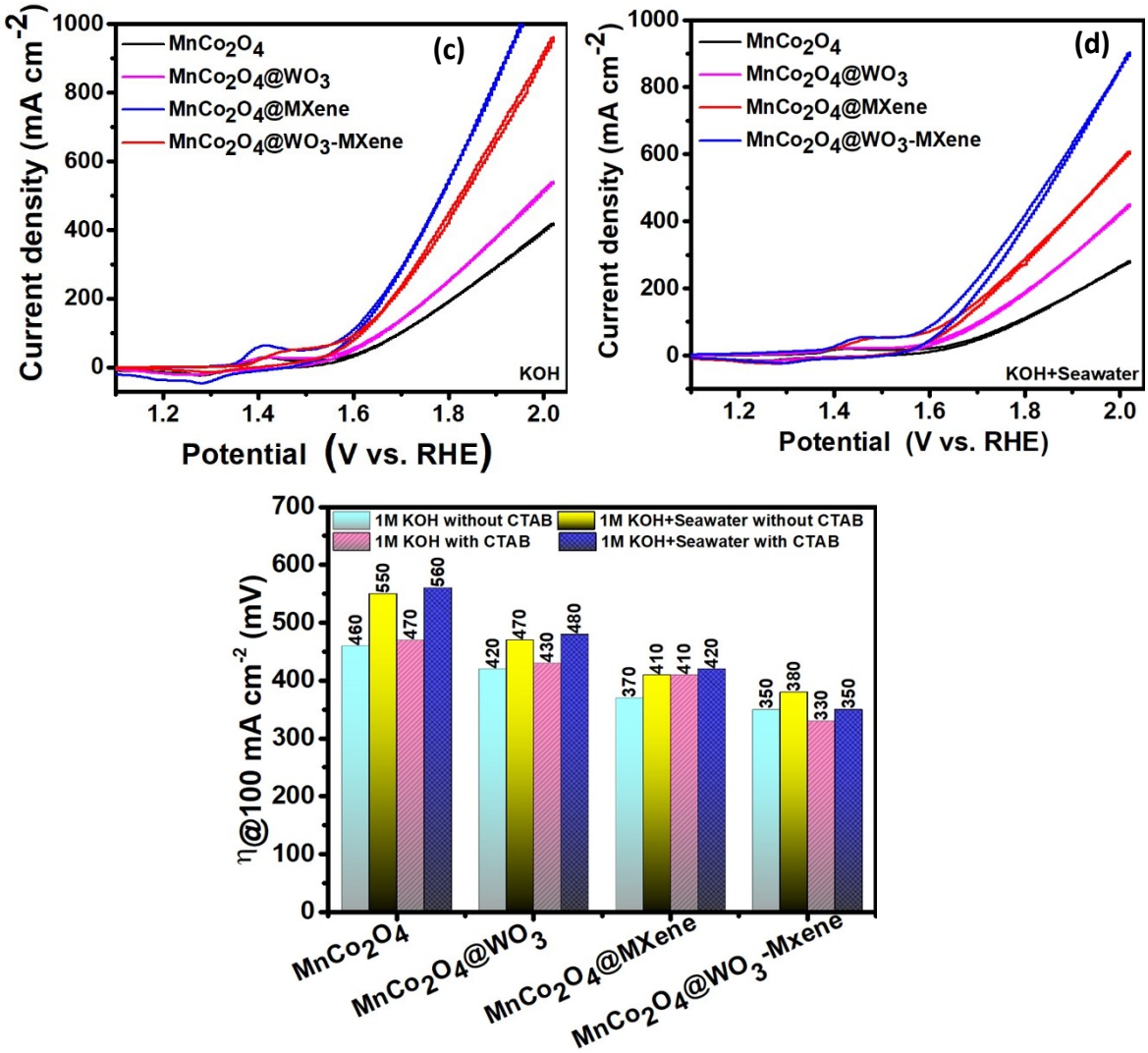

Figure S9. (a) CV curve in 1M KOH, (b) CV curve in alkaline seawater, and (c) overpotential graph without CTAB.

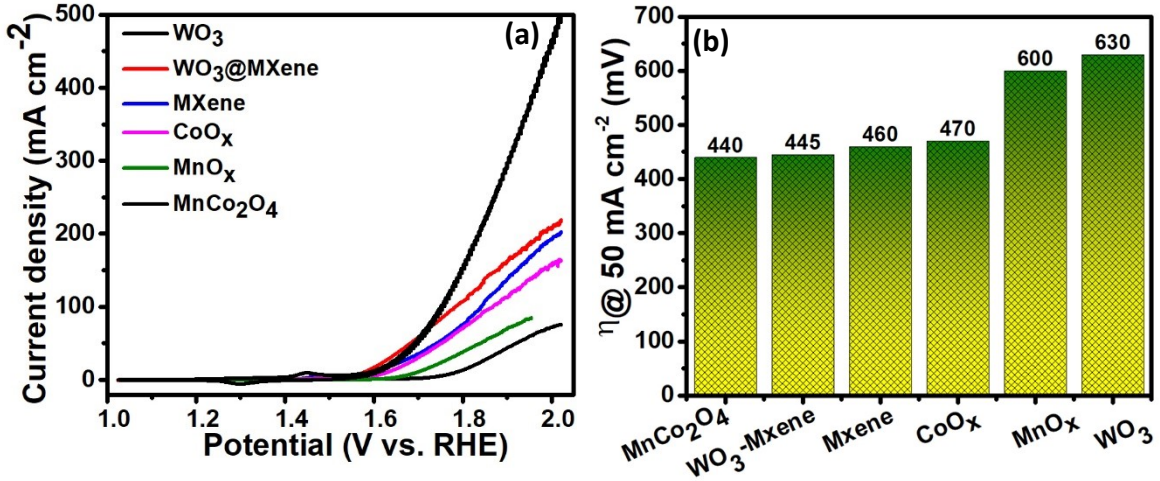

Figure S10. (a) CV curve and (b) overpotential of synthesized samples in alkaline seawater.

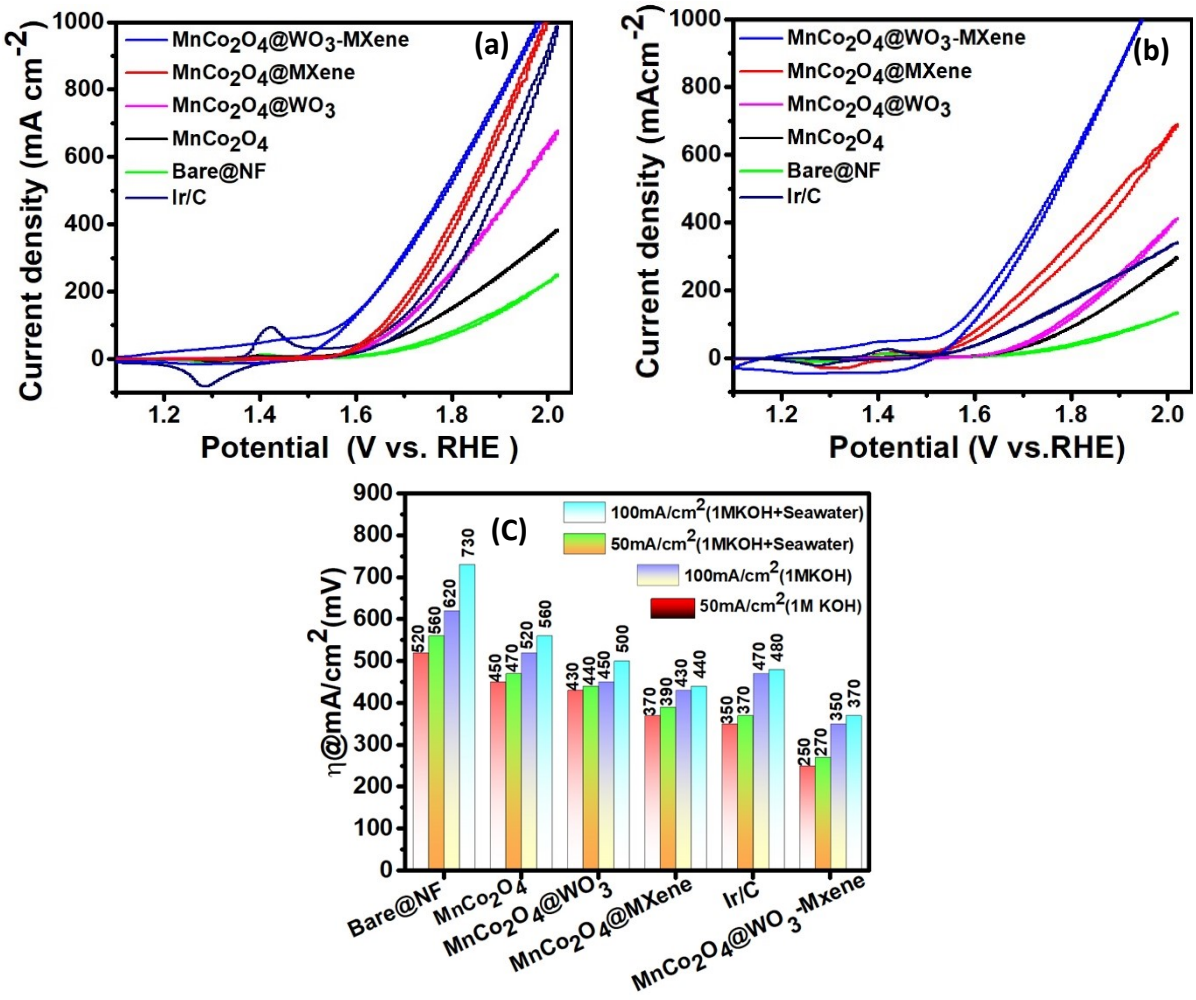

Figure S11. Without IR-corrected CV curve of $MnCo_2O_4$@WO_3-MXene at a scan rate of 5 mV/s in **(**a) 1M KOH and (b) alkaline seawater. (c) Without IR-corrected overpotential of synthesized samples in 1M KOH and alkaline seawater.

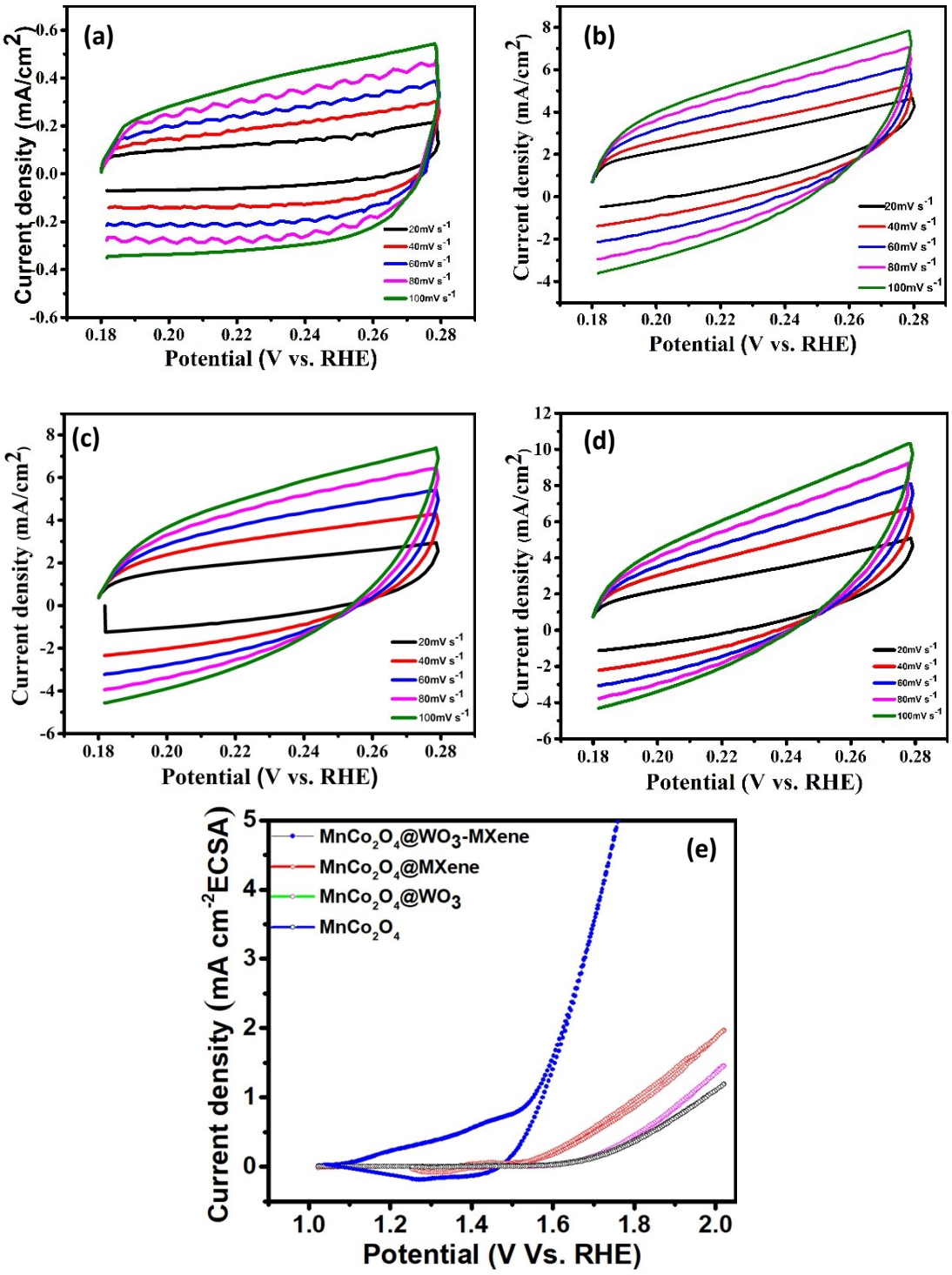

Figure S12. CV graphs of (a) $MnCo_2O_4$, (b) $MnCo_2O_4$-WO_3, (C) $MnCo_2O_4$-MXene, (d) $MnCo_2O_4$-WO_3-MXene, (e) ECSA-normalized polarization curves of the prepared samples.

Table S9: Cdl and ECSA calculation with CV curves for $MnCo_2O_4$, $MnCo_2O_4$@WO_3, $MnCo_2O_4$@MXene, and $MnCo_2O_4$-WO_3- MXene

Parameters	C_{dl} (mF)	ECSA (cm^2)
$MnCo_2O_4$	10.06	251.5

$MnCo_2O_4$@WO_3	11.25	281.16
$MnCo_2O_4$@MXene	11.36	284.08
$MnCo_2O_4$-WO_3- MXene	11.7	292.47

Calculation of ECSA:

The ECSA of the catalyst is calculated from the double-layer capacitance according to the following equation: 1.

$$ECSA = \frac{C_{dl}}{C_s} \quad (1)$$

Where Cs is specific capacitance per unit area. The typical value of specific capacitance is 40 μF/cm^2 in 1M KOH and alkaline seawater solution, as reported in literature.

Calculation of TOF: The turnover frequency (TOF) can be calculated from the following equation:

$$TOF = j \times A/(4 \times F \times n)$$

Where j is the current density (A cm^{-2}), A is the electrode area, 4 corresponds to the four-electron oxygen evolution reaction, F is the Faraday constant (96485.3 C mol^{-1}), and n is the number of moles of active material on the substrate. The value of n was calculated based on the catalyst loading mass and its molecular weight [1]. Because the exact nature and number of active sites are not fully understood, the number of active sites was estimated using ECSA for CoMnOx@WO_3-MXene. In this estimation, each metal cation (Co or Mn) was assumed to represent one active site, which may lead to an underestimation of the actual TOF.

Calculation of Mass activity: To calculate mass activity (A g^{-1}), the catalyst's loading density m and the measured current density j (mA cm^{-2}) at η=1.55 V. The equation for mass activity is as follows.

$$\text{Mass activity} = j/m$$

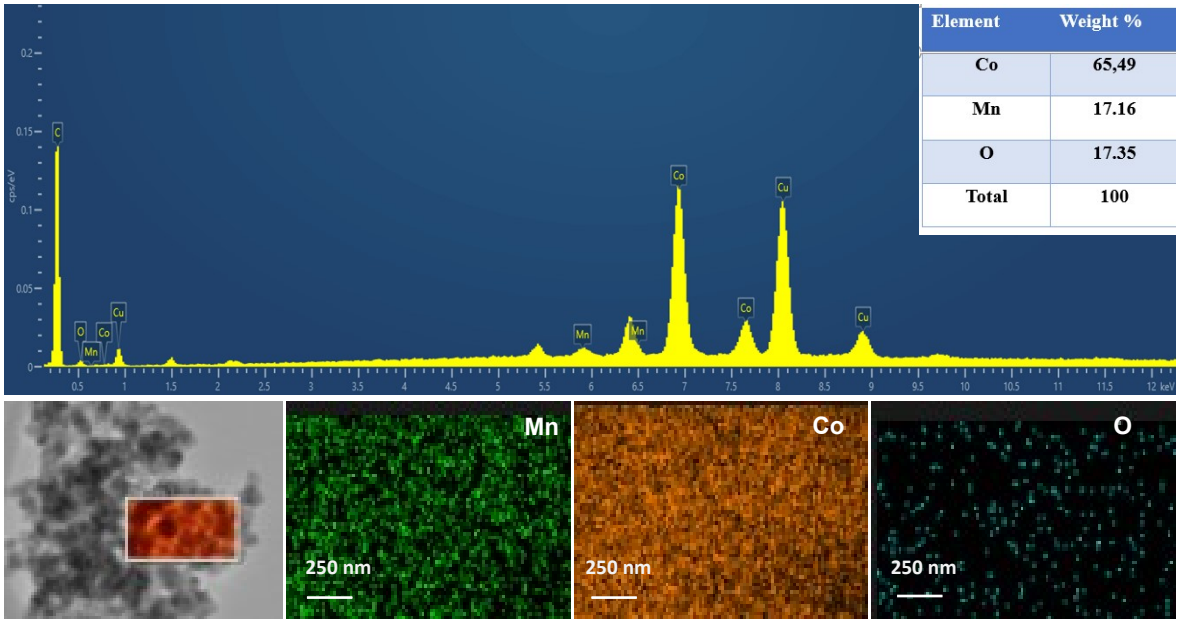

Figure S13. EDS mapping of CoMnOx. (inset shows the weight percent of the composition).

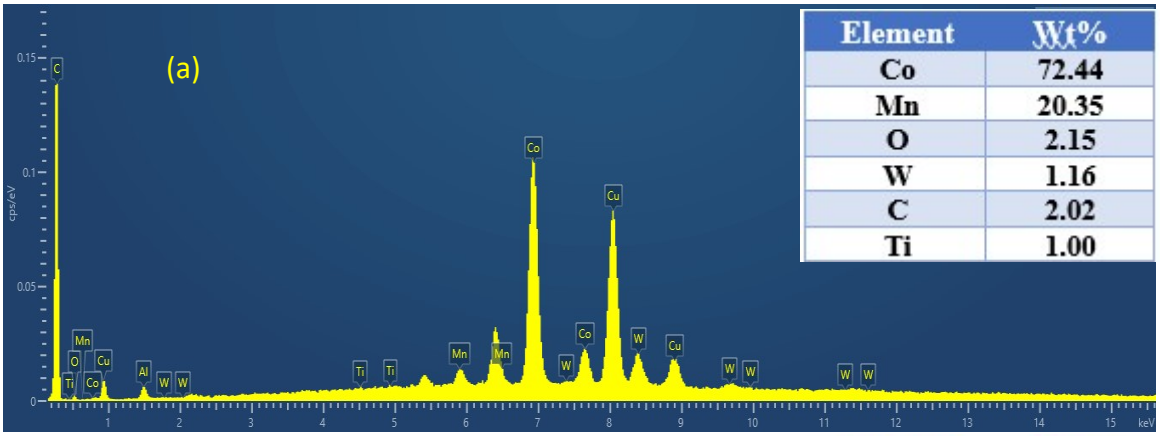

Element	Wt%
Co	72.44
Mn	20.35
O	2.15
W	1.16
C	2.02
Ti	1.00

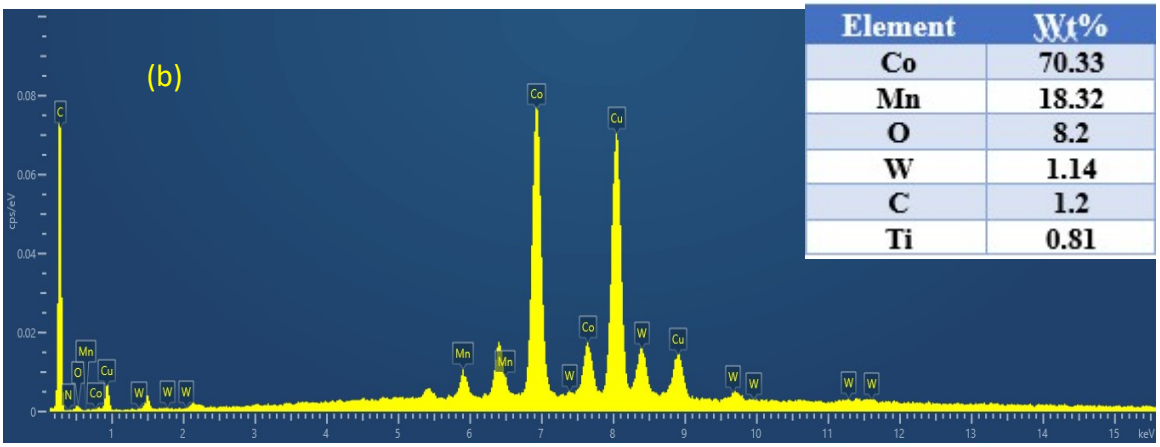

Element	Wt%
Co	70.33
Mn	18.32
O	8.2
W	1.14
C	1.2
Ti	0.81

Figure S14. EDS mapping of CoMnOx@WO3-MXene (a) before and (b) after a 100-hour stability test. (inset shows the weight percent of the composition).

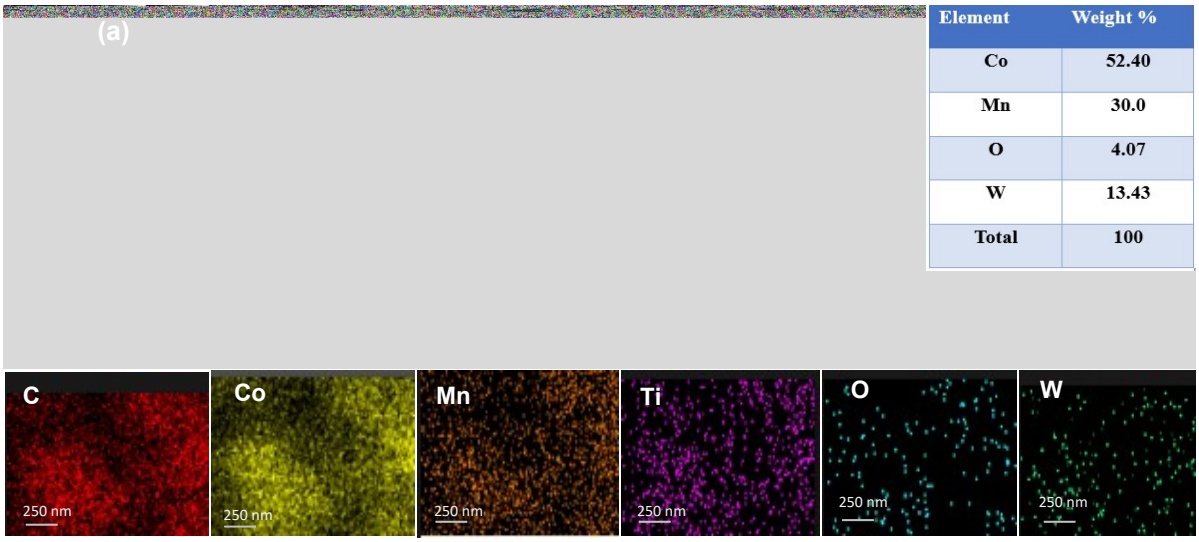

Element	Weight %
Co	52.40
Mn	30.0
O	4.07
W	13.43
Total	100

Figure S15. EDS mapping of CoMnOx@WO_3 (inset shows the weight percent of the composition).

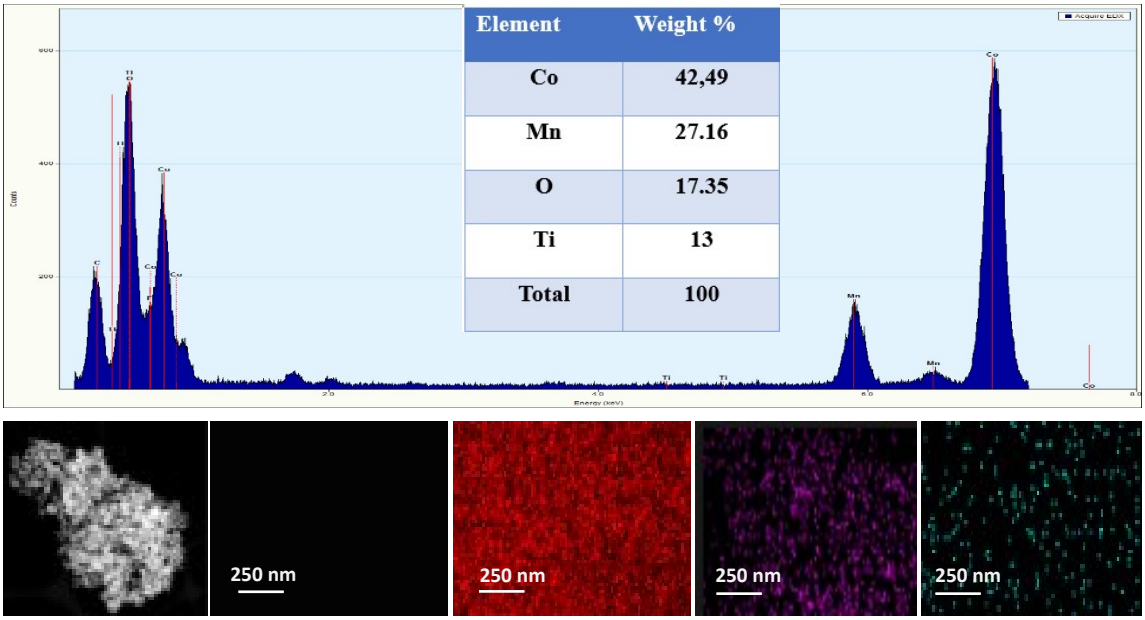

Element	Weight %
Co	42,49
Mn	27.16
O	17.35
Ti	13
Total	100

Figure S16. EDS mapping of CoMnOx@MXene. (inset shows the weight percent of the composition).

Table S10. Post stability ICP-OES data

S.No.	Co (pbb)	Mn (pbb)	W (pbb)	Ti (pbb)
1	22.725	24.503	3.12	4.26
2	21.370	24.985	3.05	4.01
Mean	22.0475	24.744	3.085	4.135
Standard deviation	0.95	0.34	0.04	0.17

Co-precipitation method for large-scale production:

In this current work, the samples were synthesized using the facile co-precipitation method. The method is suitable for large-scale production due to its simplicity, use of solution-based processing, and need for low energy. The precursors used are inexpensive and widely used commercially. The overall synthesis process is highly cost-effective. The reaction is carried out without the need for high pressure and does not need specialized equipment or any complex multistep procedure. making this method easy to use.

Precursor cost:

The precursors used in the synthesis process, such as cobalt nitrate, manganese nitrate, NaOH (sodium hydroxide), and WO_3 (tungsten trioxide), are inexpensive and commercially available in bulk. Maxine is relatively more costly but used in a small quantity. To prove the cost-effectiveness of the synthesized sample, the cost of the catalyst is compared with the state-of-the-art OER catalyst. The overall cost of all precursors is around 200-230/g for lab synthesis. This cost could be extensively reduced with bulk production. In contrast, the same quantity of RuO_2 costs around 6,000-9,000, and IrO_2 will cost 12,000-18,000.

Catalyst	Composition	Average cost/gram	Remark
RuO2	Nobel metal	5000-8000	Very high cost Scarcity
IrO2	Nobel metal	11000-15000	High cost Stability issue
$MnCo_2O_4$@WO_3-MXene	Non-Nobel metal	200-230	Low cost

Reproducibility:

In terms of reproducibility, the coprecipitation method is an excellent option. With reaction parameters such as temperature, precursor concentration, and pH, the process can easily be controlled for reproducibility for large batches.

Challenges:

- **Need of CTAB:** To corroborate the importance of the CTAB surfactant, the $MnCo_2O_4$@WO_3-MXene was synthesized with and without CTAB and investigated for its corresponding OER performance. The HRTEM image (Figure S8) reveals a significant increase in particle size for the catalyst synthesized without CTAB as compared to the CTAB-assisted samples. The results exhibit that the CTAB acts as a very essential surfactant and effectively controls morphology and prevents particle agglomeration. The electrochemical analysis (Figure S9) demonstrates that, in 1M KOH, the overpotential decreases from 350 mV (without CTAB) to 330 mV (with CTAB) to achieve a current density of 100 mA/cm^2, while in seawater, the overpotential decreased from 380 mV (without CTAB) to 350 mV (with CTAB) to achieve the same current density. Similar trends have been followed by the other samples. The improved performance can be attributed to the role of CTAB as a structure-directing surfactant, which facilitates nucleation and growth, promotes uniform nanocube formation, and prevents particle agglomeration during synthesis to ensure better distribution on the MXene sheet. In addition, the use of CTAB during the synthesis improves the product yield.

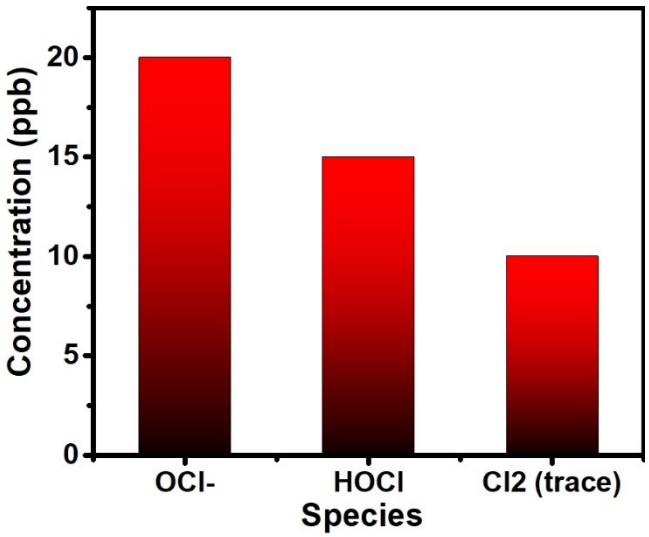

Figure S17. UPLC-MS quantified concentration of chlorine-containing species after stability alkaline seawater electrolysis.

Table S11: Literature review to compare the performance of different catalysts

Our work in 1 M KOH and 1 M KOH + seawater is compared to recent OER electrocatalysts.

S. N.	Catalyst	Electrolyte	J mA cm^{-2}	η (mV)	Stability (hours)	Refe
1	Ru/NiO	1 M KOH 1 M KOH +seawater	50	240 400	100 hours at 100 $mAcm^{-2}$	[2]
2	Nb-WO_3/WS_2	1 M KOH +seawater	50	320	100 hours at 100 $mAcm^{-2}$	[3]
3	$NiCo_2O_4$/MXene	1 M1 KOH	50	390	14 hours	[4]
4	$MnCo_2O_4$@CoS hybrid	1 M KOH 1 M KOH seawater	50	270 350	50 hours at 100 $mAcm^{-2}$	[5]
5	S-HEO/rGO	1 M KOH 1 M KOH seawater	50	320 370	100 hours at 10 $mAcm^{-2}$	[6]
6	NiCoP nano needle grown on $Ti_3C_2T_x$	1 M KOH	50	303	50 hours at 50mA cm^{-2}	[7]
7	NiHf-LDH/MXene/NF	1 M KOH 1 M KOH seawater	50	230 290	150 hours at 100 mA cm^{-2}	[8]
8	CeMnCo2O4	11 M KOH	50	420	50 hours at 10 mA cm^{-2}	[9]
9	CeO*x*@NiCo2O4 Arrays	1 M KOH 1 M KOH +seawater	50	290 300	60 hours at 100 $mAcm^{-2}$	[10]
10	B-Co2Fe LDH	1 M KOH 1 M KOH +seawater	50	220 290	100 hours at 500 $mAcm^{-2}$	[1]
11	MoO3/Fe2O3/MoS2	1 M KOH 1 M KOH +seawater	50	290 340	100 hours at 300 $mAcm^{-2}$	[11]
12	$CuCo_2O_4$/$Ti_3C_2T_x$	1 M KOH	50	420	5 hours at 10 mA cm^{-2}	[12]
13	Co-Fe2P	1 M KOH 1 M KOH +seawater	50	250 400	20 hours at 250 mA cm^{-2}	[13]
14	$(NiCoMnCrFe)_3O_4$	1 M KOH 1 M KOH +seawater	50	240 320	160 hours at	[14]
15	$(FeCoNiMnCr)_3O_4$	1 M KOH 1 M KOH +seawater	50	323 348	60 hours at 100 $mAcm^{-2}$	[15]
16	$MnCo_2O_4$@WO3-MXene	1 M KOH 1 M KOH +seawater	50	230 250	100 hours at 500 $mAcm^{-2}$	In this work

[1] L. Wu, L. Yu, Q. Zhu, B. McElhenny, F. Zhang, C. Wu, X. Xing, J. Bao, S. Chen, Z. Ren, Boron-modified cobalt iron layered double hydroxides for high efficiency seawater oxidation, Nano Energy, 83 (2021) 105838.
[2] H. Luo, T. Zhou, R. Xia, Z. Guo, Reconstructed Monolithic RuNi Heterostructure Enables Hydrogen Production from Alkaline Seawater at Industrial Current Density, Advanced Science, 12 (2025) e10916.
[3] L. Yang, Z. Xing, Y. Chen, M. Yang, W. Liu, K. Qin, X. Sun, Q. Li, M. Xiao, Z. Jia, Anion Shielding in Nb-WO3/WS2 Heterostructures: A Strategy for Efficient and Corrosion-Resistant Seawater Electrolysis, Small, 21 (2025) e09761.
[4] A. Vazhayil, L. Vazhayal, S. Ashok C, J. Thomas, N. Thomas, NiCo2O4/MXene hybrid as an efficient bifunctional electrocatalyst for oxygen evolution and reduction reaction, ChemCatChem, 16 (2024) e202301250.
[5] M.A. Khan, Y. Liu, M. Hayat, F. Lu, M. Zhou, Tuning the sulfide interface of MnCo2O4-based nanostructures enables efficient water/seawater electrolysis, International Journal of Hydrogen Energy, 89 (2024) 1-9.
[6] Y.S.S. Sarma, A. Ghosh, M. Jaiswal, S. Bhattacharya, S. Ramaprabhu, A spinel based high entropy oxide (Co, Fe, Mn, Ni, Li) 3O4 and reduced graphene oxide composite anode for seawater electrolysis, International Journal of Hydrogen Energy, 130 (2025) 54-63.
[7] M. Jeong, S. Park, T. Kwon, M. Kwon, S. Yuk, S. Kim, C. Yeon, C.-W. Lee, D. Lee, Interface Engineering via Ti3C2T x MXene Enabled Highly Efficient Bifunctional NiCoP Array Catalysts for Alkaline Water Splitting, ACS Applied Materials & Interfaces, 16 (2024) 34798-34808.
[8] D. Chauhan, M. Itagi, Y.-H. Ahn, Seawater electrolysis incorporating NiHf-LDH/MXene/NF high-performance electrocatalysts, International Journal of Hydrogen Energy, 198 (2026) 152735.
[9] X. Huang, H. Zheng, G. Lu, P. Wang, L. Xing, J. Wang, G. Wang, Enhanced water splitting electrocatalysis over MnCo2O4 via introduction of suitable Ce content, ACS Sustainable Chemistry & Engineering, 7 (2018) 1169-1177.
[10] W. Liu, J. Zhao, L. Dai, Y. Qi, K. Liang, J. Bao, Y. Ren, Interface Engineering Overall Seawater Splitting of Self-Supporting CeO x@ NiCo2O4 Arrays, Inorganic Chemistry, 63 (2024) 6016-6025.
[11] Z. Li, W. Tao, Y. Wang, X. Ye, Y. Chen, B. Han, L.Y.S. Lee, Corrosion-Resistant MoO3/Fe2O3/MoS2 Heterojunctions Stabilize OH–Adsorption for Efficient Light-Assisted Seawater Electrooxidation, Journal of the American Chemical Society, 147 (2025) 24461-24472.
[12] S. Ghorbanzadeh, S. Hosseini, M. Alishahi, CuCo2O4/Ti3C2Tx MXene hybrid electrocatalysts for oxygen evolution reaction of water splitting, Journal of Alloys and Compounds, 920 (2022) 165811.
[13] S. Wang, P. Yang, X. Sun, H. Xing, J. Hu, P. Chen, Z. Cui, W. Zhu, Z. Ma, Synthesis of 3D heterostructure Co-doped Fe2P electrocatalyst for overall seawater electrolysis, Applied Catalysis B: Environmental, 297 (2021) 120386.
[14] J. Fan, X. Xiang, Y. Liu, X. Yang, N. Shi, D. Xu, C. Zhou, M. Han, J. Bao, W. Huang, Defect-rich high-entropy spinel oxide as an efficient and robust oxygen evolution catalyst for seawater electrolysis, SusMat, 5 (2025) e70010.
[15] B. Du, J. Zeng, R. Tang, Y. Li, Q. Hao, F. Wang, L. Liang, H. Liu, High-entropy spinel (FeCoNiMnCr) 3 O 4 nanoparticles supported on carbon nanotubes for enhanced electrochemical seawater oxidation, Chemical Communications, 61 (2025) 15614-15617.